JOURNAL OF CATALYSIS 67, 49–70 (1981)

The Adsorption of Formic Acid on Y Zeolites: A Multiple-Pulse Nuclear Magnetic Resonance Study

T. M. DUNCAN[1] AND R. W. VAUGHAN[2]

Division of Chemistry and Chemical Engineering, California Institute of Technology, Pasadena, California 91125

Received March 19, 1980; revised July 28, 1980

A series of multiple-pulse nuclear magnetic resonance (NMR) techniques have been applied to the study of the adsorbed state of formic acid on ammonium–Y (NH_4–Y) and ultrastable hydrogen–Y (H–Y) zeolites. It is determined that the formic acid is adsorbed on the zeolites in two different forms: as unidentate and bidentate formate species, which can be distinguished by the symmetry of the ^{13}C chemical shift powder patterns. Cross-polarization NMR techniques exploit differences in the ^{13}C–^{1}H dipolar couplings to separate the two groups. The ratio of bidentate to unidentate species is about 52 : 48 on the NH_4–Y zeolite and about 83 : 17 on the ultrastable H–Y zeolite at a coverage of 0.3 monolayer. The strength of the ^{13}C–^{27}Al dipolar interaction suggests that the bidentate formate ions are bonded to the Al atoms of the zeolites. The ^{1}H NMR spectrum of the carbonyl hydrogen, isolated by a dipolar-difference technique, is shifted downfield from that of neat formic acid, indicating that the hydrogen has become more acidic.

I. INTRODUCTION

The adsorbed state of formic acid on metal oxides has been studied by various spectroscopic techniques, primarily transmission infrared (*1–4*). Other studies include inelastic electron tunneling spectroscopy (*5, 6*) and high-resolution nuclear magnetic resonance (NMR) methods (*1*). We present here a multiple-pulse NMR study of the nature of formic acid adsorbed on two Y zeolites (Si/Al = 2.8): an ammonium–Y (NH_4–Y) and an ultrastable hydrogen–Y (H–Y) zeolite.

Both zeolites have the faujasite-type structure containing nearly spherical cavities 12 Å in diameter interconnected by 8- to 9-Å openings (*7*). The ultrastable H–Y is the "deep-bed" calcination product of the NH_4–Y zeolite at about 775 K (*8*). Although derived from the NH_4–Y zeolite, the ultrastable H–Y zeolite is quite different, possessing increased catalytic properties with respect to Brønsted acid-catalyzed reactions such as alkylation and hydrocarbon cracking, increased thermal stability, and increased resistance to decomposition (*9*). It is proposed that the increased stability is in part the result of the removal of a portion of the tetrahedrally coordinated framework Al atoms, yielding cationic Al species with charges ranging from 1 to 3 (*10*). Specifically, it is suggested that the decomposition of the NH_4–Y to the ultrastable H–Y zeolite creates 9 to 15 Al cations per unit cell (*10*). This is consistent with ammonia adsorption studies on the ultrastable H–Y zeolite which indicate the presence of 12 new Brønsted acid sites per unit cell (*10*). However, although it is generally accepted that the results of chemical analysis and X-ray diffraction suggest an aluminum-deficient structure, the nature of the nonframework aluminum and the defect site is still uncertain (*11*).

Formic acid adsorbs irreversibly on both zeolites. Upon desorption, submonolayer coverages of formic acid decompose almost exclusively to CO and H_2O. It is the general conclusion of the studies cited above that the formic acid chemisorbs onto metal oxides via the loss of the acidic hydrogen. The

[1] Present address: Bell Telephone Laboratories, Murray Hill, N.J. 07974.

[2] Deceased.

0021-9517/81/010049-22$02.00/0

formate ion is then bonded to the substrate through one or both of the oxygen atoms. The state of the formate ion may be described by any one, or a combination, of the species shown below.

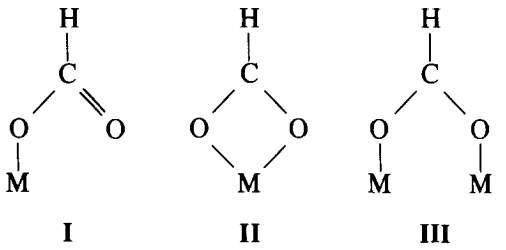

The unidentate formate structure (species **I**) is bonded through a single oxygen atom, as in formic acid and formate esters. The bidentate and bridging bidentate structures (species **II** and **III**) may occur in both symmetrical and unsymmetrical forms, depending on the metal ion lattice spacings. Infrared studies on formate salts suggest that the formate bonding is determined by the ionic radius of the metal atom (*12*), the electronegativity of the metal (*13*), or both properties plus the mass of the metal atom (*14*).

Because of the lack of periodicity and low concentrations of surface formate species on the polycrystalline zeolite samples, it is not feasible to determine directly the structure of the adsorbate by various diffraction methods (*15*). It is, therefore, necessary to examine other quantities which are sensitive to the molecular geometry and then, through analogy with known structures, determine the state of the adsorbed species. In this paper we examine one such property, the chemical shift tensor of the adsorbed formic acid, with multiple-pulse NMR techniques.

The application of NMR techniques to the study of adsorbed species has been discussed in several reviews (*16–18*). Although there have been numerous NMR studies of physically adsorbed hydrocarbons, there have been relatively few applications to the study of chemically adsorbed species. Examples of chemically adsorbed systems include the study of benzene on charcoal and silica gel (*19*), carbon dioxide on molecular sieves (*20*), and carbon monoxide on rhodium on alumina (*21*). One difficulty with NMR studies of chemisorbed molecules is the extremely weak NMR signals of such dilute systems, which is further complicated by excessive broadening. To date, most studies on physically adsorbed molecules have concentrated on the spin–lattice relaxation times and the isotropic frequency of the resonance. This study will concentrate more on the anisotropic chemical shift tensor and the dipolar interaction between the ^{13}C nuclei and neighboring nuclei, two quantities which are averaged-out in physically adsorbed systems. These interactions will be used to determine the geometry of the adsorbed state, the degree of motion on the surface, and the nature of the adsorption site.

This study will utilize several high-resolution NMR pulse sequences (*22–24*), including spin-decoupling (*25*), cross-polarization (*25, 26*), dipolar-modulation (*27*), and dipolar-difference (*28*) techniques to enhance the NMR signals and attenuate the extraneous broadening. The analysis will be based primarily on ^{13}C NMR spectra. The ^{13}C nuclei are a dilute spin system in the zeolite and interact almost exclusively through other spin systems or the lattice; thus, there is negligible broadening from homonuclear interactions. The ^{13}C chemical shifts are much larger than those of ^{1}H

nuclei, which allows an interpretation of the spectra even in the presence of substantial broadening. The ^1H spectrum of the carbonyl hydrogen of formic acid will be measured also as a cross-reference on the environment of the adsorbed species.

The NMR pulse techniques will be used to measure the chemical shift tensor, the dipolar interactions with ^1H and ^{27}Al nuclei, and the various relaxation times of the ^{13}C nuclei of the adsorbed formic acid. The center-of-mass of the chemical shift tensor (the isotropic value observed in physically adsorbed samples) reflects the general character of the chemistry of the molecular species; that is, the isotropic chemical shift readily distinguishes between fundamentally different carbon compounds such as carbonyl, aliphatic, and aromatic groups. However, the isotropic value is not a good indicator of subtle chemical differences within a subgroup such as the formate compounds (*29*). Rather, the changes in bonding geometry are better reflected by the anisotropy of the chemical shift tensor. In general, within a subgroup the isotropic value indicates the average electron density at the ^{13}C nucleus, whereas the full tensor is sensitive to changes in the angular distribution and symmetry of the electron density.

The interaction of the ^{13}C nuclei with neighboring dipoles can be used to determine average internuclear distances and the extent of motional averaging. The ^{13}C nuclei are most strongly coupled to the nuclei of the directly bonded hydrogen atoms. Thus, it is possible to apply cross-polarization techniques to study the strength of the coupling (*26*) and to enhance the ^{13}C NMR spectrum (*25*). The interaction may be used to isolate the ^1H NMR spectrum of the carbonyl proton from the broad, diffuse lineshape of the other protons of the sample (*28*). The extent of the ^{27}Al broadening of the ^{13}C NMR spectrum provides an estimate of the ^{13}C–^{27}Al internuclear distance and, thus, information on the adsorption site of the formic acid.

The three time constants measured in this study are the spin–lattice relaxation time (T_1), the transverse relaxation time (T_2), and the time constant for the coupling between the ^{13}C and the ^1H spin baths (T_{IS}). The T_1 is the time constant for the rate that the perturbed magnetization returns to equilibrium with the external magnetic field. In samples with relatively high paramagnetic impurity levels, as is the case with the two zeolites studied here, the T_1 of a chemisorbed species cannot be used to determine the nature of the motion on the surface or the cross-relaxation rate with neighboring spins. However, in some cases the T_1 may be used to differentiate between various adsorbed states by the nature of the coupling to the paramagnetic centers (*21*). T_2 is essentially the lifetime of the spin state, which is often limited by motions of the molecule or motions of nearby unpaired electrons of paramagnetic centers. T_{IS} is measured by the rate at which the magnetization is transferred between the ^{13}C and the ^1H spin systems and may be used to calculate the strength of the dipolar interaction.

II. EXPERIMENTAL PROCEDURE

A. Sample Description and Preparation

The NH_4–Y zeolite, unit cell formula $Na_2(NH_4)_{48}(AlO_2)_{50}(SiO_2)_{142} \cdot 267H_2O$, was prepared by ion exchange with a sodium–Y zeolite. This NH_4–Y zeolite was calcined at 775 K to yield a "deep-bed" product, an ultrastable H–Y zeolite, with unit cell formula $Na_2H_{48}(AlO_2)_{50}(SiO_2)_{142} \cdot 26H_2O$ (*8, 10*). The zeolites contain 780 ± 10 ppm Fe and 12 ± 2 ppm Mn, as determined by atomic absorption. The electron paramagnetic spectra of the zeolites at 8 K and the microwave frequency at 9.25 GHz show a sharp transition at $g = 4.4$ and a multiplet of about six transitions ranging from $g = 2.2$ to 1.9. The sharp line at $g = 4.4$ is typical of Fe^{2+} in silica–aluminas, whereas the multiplet at about $g = 2.0$ is indicative of Mn^{2+} (*30*). The sharpness of the transitions indicates that the paramagnetic centers are

atomically dispersed in the zeolites and not clustered in metallic particles.

The zeolite samples were outgassed with a liquid-nitrogen-trapped diffusion pump to pressures of about 5×10^{-5} Torr (1 Torr = 133.3 N/m^2) by heating for 3 hr: the NH_4–Y zeolite at 385 K and the ultrastable H–Y at 800 K. The nitrogen BET surface areas of the zeolites are 459 ± 10 and 515 ± 10 m^2/g for the NH_4–Y and the ultrastable H–Y, respectively, representing monolayers of about 63 and 84 nitrogen molecules per unit cell. The formic acid adsorption isotherms for both zeolites, shown in Fig. 1, reveal monolayer coverages of 75 and 56 formic acid molecules per unit cell, or 5.7×10^{14} and 5.5×10^{14} molecules/cm^2, for the NH_4–Y and the ultrastable H–Y zeolites, respectively. The formic acid was adsorbed from the gas phase. The predetermined pressure of the vapor to be adsorbed was calculated from the monomer/dimer equilibrium data of Coolidge (*31*). The continuous uptake of formic acid by the NH_4–Y zeolite for P/P_0 greater than 0.22 suggests that the zeolite is decomposing under acid attack. The ultrastable H–Y exhibits no such degradation in the pressures studied ($P/P_0 < 0.5$). For coverages less than 40 molecules per unit cell, the equilibrium pressure of the formic acid was less than 0.1 Torr, below the range of the Wallace and Tiernan gauge used in the adsorption studies. A mass spectrometric analysis of the formic acid desorption products from a submonolayer coverage on the ultrastrable H–Y at 525 K revealed that the carbon was evolved as 98.5% CO and 1.5% CO_2 with no trace on any residual formic acid detected.

This NMR study was performed on two samples of zeolites with submonolayer coverages of isotopically enriched (91.2% ^{13}C) formic acid. Quantitatively, one sample consisted of 0.120 g of NH_4–Y zeolite loaded with 1.81×10^{-4} mole (9.9×10^{19} ^{13}C nuclei) of formic acid, a coverage of 24.9 molecules of formic acid per unit cell of zeolite. The second sample was 0.121 g of ultrastable H–Y zeolite dosed with 1.86×10^{-4} mole (1.02×10^{20} ^{13}C nuclei) of formic acid, a coverage of 18.5 molecules of formic acid per unit cell. We are confident that the structural integrity of the NH_4–Y zeolite is maintained under this light loading of the acid. The acid coverage is significantly below the point where the anomalies occur in the adsorption isotherm and the ratio of hydrogen ions to ammonium ions is low, an

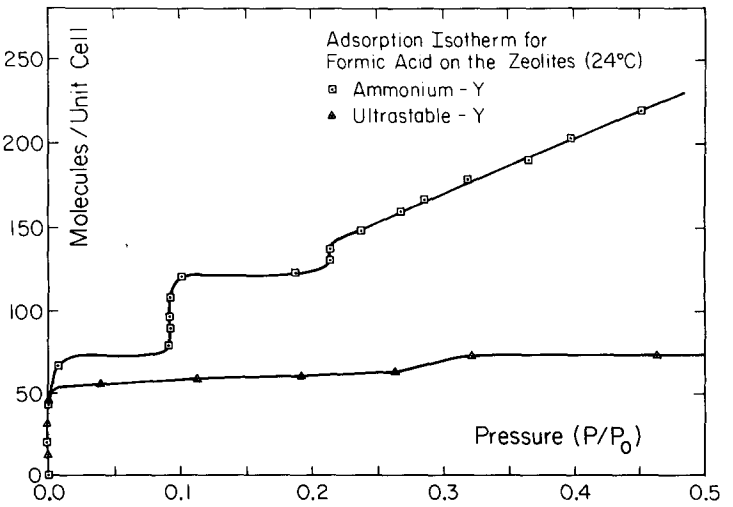

FIG. 1. Adsorption isotherms for formic acid on the NH_4–Y (□) and the ultrastable H–Y (△) zeolites at 297 K.

important criterion for zeolite stability (*32*).

The ^{13}C NMR spectra of the reference compounds were obtained from enriched samples of formic acid, ammonium formate, and calcium formate. The formic acid sample was 20% ^{13}C-enriched, prepared by diluting the 91.2% stock with natural-abundance formic acid. The ammonium formate sample (12% ^{13}C-enriched) was prepared by neutralizing the formic acid with ammonium hydroxide and then vacuum-desiccating to remove the residual water and ammonia. The calcium formate reference, examined previously (*27*), contained 6% ^{13}C and was doped with Mn^{2+} to lower spin–lattice relaxation times.

B. NMR Spectrometer and Pulse Sequences

The Fourier transform ^{13}C and ^{1}H NMR spectra were measured on a double-resonance multiple-pulse spectrometer (*33, 34*). The 1.32 Tesla Varian magnet is stabilized to about 1 ppm with an external ^{19}F pulsed field-frequency lock. The data were taken with a single-coil (5-mm diameter) double-resonance probe tuned for ^{1}H resonance at 56.4 MHz and ^{13}C resonance at 14.2 MHz (*34*). Temperatures were regulated by a dewared nitrogen flow system.

The ^{13}C NMR spectra in this study were obtained by Fourier transforming the signals observed with three techniques: the 180°–τ–90° (*35*), ^{13}C–^{1}H cross-polarization (*25*), and ^{13}C–^{1}H dipolar-modulation (*27*) experiments. The ^{1}H spectrum of the carbonyl proton was observed by the ^{13}C–^{1}H dipolar-difference experiment (*28*). These four pulse sequences are diagramed in Fig. 2. The intensities and lineshapes of the NMR spectra as a function of the various parameters of each pulse sequence can be used to describe the adsorbed state and the local environment of the formic acid. The main features of each pulse scheme will be described briefly. More extensive discussions may be found in the reviews mentioned earlier (*22–24*).

The 180°–τ–90° pulse sequence measures quantitatively the number of ^{13}C nuclei in the sample; provided that $T_1 \gg \tau$, the sequence is repeated only after waiting a period of at least five T_1's, and the proton irradiation is sufficiently intense to decouple the ^{13}C–^{1}H spins. The criterion for heteronuclear decoupling is that the decoupling field is greater than both the ^{13}C–^{1}H heteronuclear coupling and the ^{1}H–^{1}H homonuclear spin coupling (*23*); that is, the Larmor frequency of the protons in the decoupling field must be comparable to the spin-flip rate of the protons caused by both the ^{13}C nuclei and the other protons. The Larmor frequency of the protons in a holding field of 16 G is 68 kHz. The ^{13}C–^{1}H coupling for a bond length of 1.09 Å is less than 45 kHz at the most intense orientation and averages less than 11 kHz. The square root of the second moment of the ^{1}H spectrum of either the NH_4–Y or the ultrastable H–Y zeolite is only about 5.2 kHz at 295 K. Thus, 16 G is sufficient to assure reliable ^{13}C spin counts for the adsorbed formic acid. The intensity of the observed magnetization as a function of τ, the delay between the 180 and the 90° pulses, may be used to calculate the T_1 of the ^{13}C nuclei (*35*). The 180°–τ–90° sequence is alternated with a single 90° pulse, and the successive free-induction decays are alternately added and subtracted. This add–subtract mode removes instrumental artifacts during the period immediately after the 90° pulse.

The ^{13}C–^{1}H cross-polarization experiment enhances the ^{13}C spectra and quantifies the strength of the heteronuclear interaction by measuring the rate of transfer of magnetization between the two spin systems (*25*). In general, it is not possible to predict the intensity of the signal from the cross-polarization experiment for an inhomogeneous system, such as the formic acid adsorbed on the zeolites, without a knowledge of internuclear distances and the degree of motional averaging. The cross-polarization process will selectively emphasize the signal from ^{13}C nuclei with the strongest couplings to the ^{1}H nuclei.

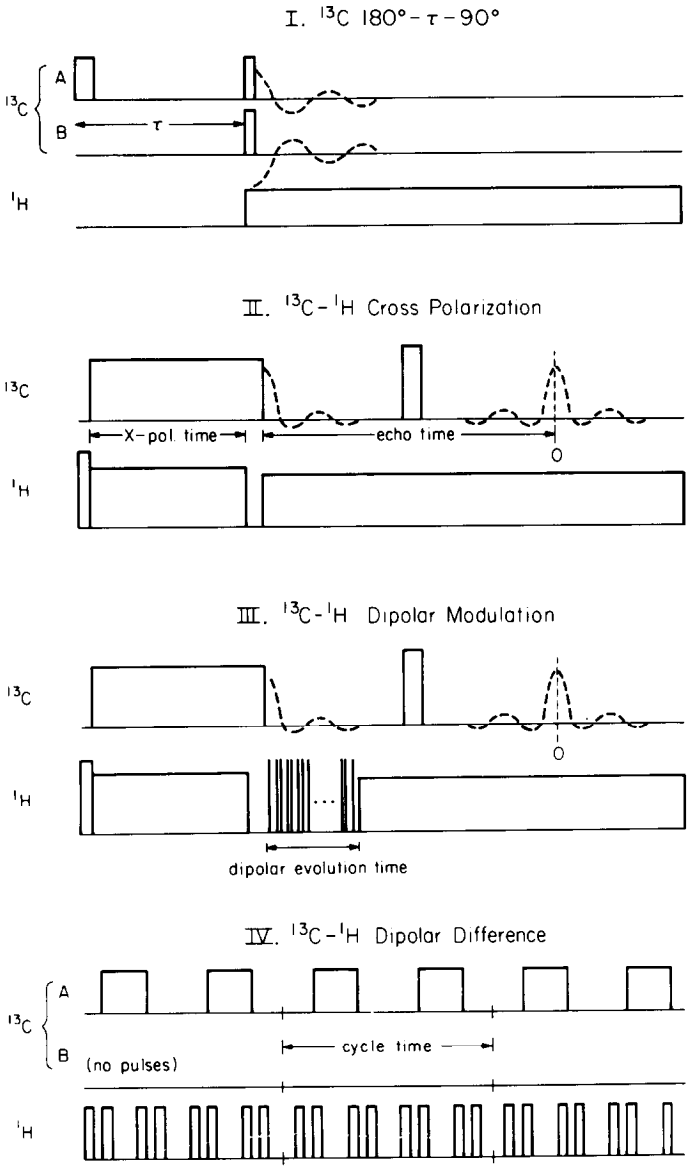

FIG. 2. Schematic representations of the NMR pulse schemes used in this study. The abscissa is time and the pulses are indicated by rectangular boxes of arbitrary height. The observed magnetization is indicated by the dashed lines. The ^{13}C and ^{1}H pulse sequences are initiated simultaneously. In the 180°–τ–90° and dipolar-difference sequences, the A and B modes of the ^{13}C sequences are applied alternately and the NMR signal is alternately added and subtracted.

The strength of the couplings depends on the number of ^{1}H spins in the immediate environment (within about 5 Å), the orientation of the ^{13}C–^{1}H vectors relative to the external magnetic field (the interaction is proportional to $(3\cos^2\theta - 1)$, where θ is the angle between the vector and the external field), and the frequency and amplitude of molecular reorientations. For ^{13}C–^{1}H bonds at orientations where the heteronuclear dipolar coupling is weak (i.e., near 55°), the ^{13}C magnetization must be produced by transfer from extramolecular protons, or ^{13}C–^{13}C homonu-

clear spin transfer. Both processes are slow and require prohibitively long ^{13}C locking fields. Thus, it is not feasible to calculate a priori the intensity of the ^{13}C cross-polarization spectra. It is, however, appropriate to compare relative signal intensities from one sample as a function of the experimental parameters.

The Hartmann–Hahn condition (*36*) for cross-polarization ($\gamma_H H_H = \gamma_c H_c$, where γ is the gyromagnetic ratio and H is the applied magnetic field) was satisfied with fields of 8.6 G at the proton frequency and 34 G at the carbon frequency. The proton decoupling was 8 G for the reference compounds and 16 G for the formic acid absorbed on the zeolites. To effect a maximum magnetization transfer, cross-polarization times ranged from 0.1 msec, for the ammonium formate at 295 K, to 8.0 msec for calcium formate at 125 K.

The better signal-to-noise ratios of the ^{13}C spectra from the cross-polarization experiment made it feasible to perform more demanding experiments such as studying the shape and intensity as a function of the cross-polarization time, the echo time, or the dipolar evolution time (*27*). As described earlier, the intensity of the magnetization as a function of the cross-polarization time is a measure of the strength of the coupling between the ^{13}C and the ^{1}H spins. The signal intensity as a function of the echo time was used to calculate the transverse relaxation time, T_2.

The ^{13}C–^{1}H dipolar-modulation experiment (*27, 37*) is a variation of the cross-polarization scheme. Immediately after the ^{13}C spin-locking pulse, a series of eight-pulse cycles (*28*) are applied to decouple the proton homonuclear interaction. However, the ^{13}C–^{1}H coupling remains although it is decreased by a factor of about 0.6. Immediately after the eight-pulse cycles, the ^{1}H decoupling pulse is turned on, which conversely decouples the ^{13}C–^{1}H interaction but not the ^{1}H–^{1}H coupling. The ^{13}C magnetization will oscillate during the eight-pulse sequence at a frequency proportional to the ^{13}C–^{1}H coupling. Thus, the extent of the modulation of the ^{13}C magnetization is determined by the strength of the ^{13}C–^{1}H coupling. With this technique it is possible in some cases to orient the chemical shift principal-axis system in the molecular coordinate system by the rate of modulation of different portions of the ^{13}C powder pattern (*27, 37*). Also, the area of the ^{13}C spectrum will oscillate at a frequency proportional to the average ^{13}C–^{1}H coupling in the sample, thus allowing one to calculate the average ^{13}C–^{1}H bond lengths.

The isolated ^{1}H chemical shift spectrum of the carbonyl hydrogen of the absorbed formic acid may be observed with the dipolar-difference experiment (*28*). In this experiment, the homonuclear-decoupled ^{1}H spectrum is observed alternately in two environments: first, using the eight-pulse cycle (*38*) to remove the ^{1}H–^{1}H interactions, and second, simultaneously irradiating the proton spins with the eight-pulse cycle while irradiating the ^{13}C nuclei to remove the heteronuclear dipolar coupling to the protons (*39*). Thus, the first cycle will yield chemical shift spectra from all protons except those bonded to ^{13}C nuclei, which will be dipolar broadened into the baseline. In the second cycle, this heteronuclear dipolar broadening is removed and all the protons are observed. Alternate adding and subtracting of these two signals yields the spectrum of only those protons bonded to ^{13}C nuclei.

The ^{13}C spin counts and resonance frequencies were calibrated with ^{13}C-enriched samples of adamantane and calcium formate. The NMR spectra are plotted on the σ scale (*23*) relative to tetramethylsilane (TMS) such that upfield is to the left. The centers-of-mass and linewidths are accurate to about ± 3.4 ppm (one channel). The lines through the spectra were obtained by a nonlinear least-squares fit of a theoretical chemical shift powder pattern (*40*). The spectra of the reference formates and the $180°$–τ–$90°$ spectra were convoluted with a Lorentzian broadening function, whereas

the cross-polarization spectra were convoluted with a Gaussian broadening function. The theoretical fits to the ^{13}C NMR spectra of the polycrystalline reference formates are accurate to ±3.4 ppm. The spectra of the adsorbed formic acid are not as well resolved and the uncertainty in the fitted chemical shift parameters is ±10 ppm (three channels).

III. RESULTS

A. ^{13}C NMR Spectra of Formate Compounds

The anisotropy and resolution of the structure of the ^{13}C NMR spectra of formic acid, ammonium formate, and calcium formate both increased as the temperature of the sample was lowered. This suggests that there are molecular motions in the crystals which are being quenched at lower temperatures. The motions are probably small anisotropic librations which cause a local averaging in the ^{13}C NMR powder patterns. In each case, the spectra were recorded at the lowest temperatures experimentally feasible, restricted by the limitations of the equipment and the temperature dependence of the spin–lattice relaxation times.

The ^{13}C NMR spectra of the reference formates shown in Fig. 3 were obtained by ^{13}C–^{1}H cross-polarizing and then observing the free-induction decay immediately after the ^{13}C spin-locking pulse, while decoupling the protons with 8 G. The principal components of the chemical shift tensors are reported in Table 1. The features in the spectrum for formic acid at 125 K, Fig. 3a, suggest three principal components of the chemical shift tensor, but the data do not fit a theoretical powder pattern lineshape. A least-squares fit, shown by the solid line, follows the upfield component at −92 ppm but clearly misses the downfield shoulder. If the three principal components are fixed at the approximate locations of the shoulders, the computed intensities at the center and downfield components are in error, as shown by the dashed line. The distortion

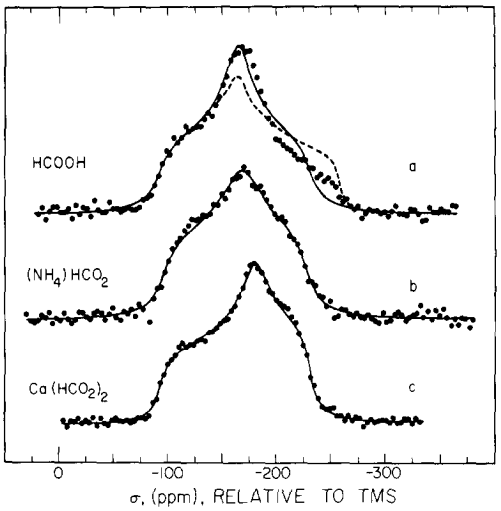

FIG. 3. ^{13}C NMR spectra of reference formates obtained by ^{13}C–^{1}H cross-polarization; (a) formic acid at 125 K, (b) ammonium formate at 185 K, and (c) calcium formate at 125 K. The abscissa scale is 3.44 ppm per point in all spectra. Frequencies are relative to tetramethylsilane (TMS).

from the theoretical lineshape is probably the result of motion as well as an angular dependence of the ^{13}C–^{1}H cross-polarization rate in a polycrystalline sample. The spectrum in Fig. 3a, obtained by cross-polarizing for 8 msec, is less distorted than the spectra that result with only 0.5 msec of ^{13}C–^{1}H spin contacting or at higher temperatures.

The spectrum for ammonium formate shown in Fig. 3b is the result of cross-polarizing for 0.1 msec at 185 K. At about 195 K, the proton T_1's lengthened from a few milliseconds to over 10 sec, which indicates that the major relaxation process had halted, probably the rapid reorientation of the ammonium ion. The proton T_1's continue to increase at temperatures below 185 K, which prohibited extended averaging.

The ^{13}C NMR spectrum of calcium formate exhibited the most pronounced motional effects of the formates studied. The apparent chemical shift anisotropy increases from about 100 ppm at 295 K to 139 ppm at 125 K. The spectrum shown in Fig. 3c was obtained by cross-polarizing for 8.0

TABLE 1

Reference Formates

A. ^{13}C chemical shift parameters

Compound	Temperature (K)	Principal components[a]			$\bar{\sigma}$	$\sigma_{33} - \sigma_{11}$	$\frac{\sigma_{22} - \sigma_{11}}{\sigma_{33} - \sigma_{11}}$	Reference
		σ_{11}	σ_{22}	σ_{33}				
$HCOOCH_3$[b]	87	−107	−136	−253	−165	146	0.20	(*41*)
HCOOH[c]	125	−92	−162	−251	−168	159	0.44	this work
$(NH_4)HCO_2$	185	−99	−168	−225	−164	126	0.55	this work
$Ca(HCO_2)_2$	125	−96	−186	−235	−172	139	0.65	this work

B. Structure

Compound	C–O bond lengths (Å)		R_2/R_1	Method	Reference
	R_1	R_2			
$HCOOCH_3$	1.22 ± 0.03	1.37 ± 0.04	1.12	electron diffraction	(*42*)
HCOOH	1.245 ± 0.002	1.312 ± 0.002	1.05	isotopic microwave	(*43*)
$(NH_4)HCO_2$	1.237 ± 0.007	1.246 ± 0.007	1.01	X-ray diffraction	(*44*)
$Ca(HCO_2)_2$[d]	1.25 ± 0.03	1.25 ± 0.03	1.00	X-ray diffraction	(*45*)
	1.24 ± 0.03	1.25 ± 0.03	1.01		

[a] In ppm, relative to tetramethylsilane (TMS).
[b] Data converted from original reference using $\sigma(C_6H_6) = -128.7$ ppm, relative to TMS (*46*).
[c] Principal components estimated from data, rather than computed lineshape.
[d] Two crystallographically distinct formate groups.

msec at 125 K. A previous ^{13}C NMR study of single-crystal calcium formate detected two distinct sets of chemical shift components for the crystallographically inequivalent formate ions (*29*). The resolution in the powder pattern of Fig. 3c is not sufficient to resolve the two spectra, which are separated by only 5, 3, and 0 ppm at the three principal components.

B. Formic Acid Adsorbed on Zeolites

1. ^{13}C T_1 Measurements

The logarithm of the calibrated amplitude of the observed ^{13}C magnetization versus the delay between the 180 and the 90° pulses is plotted in Fig. 4. If the recovery of the longitudinal magnetization were described by a single T_1, the data would lie on a straight line when plotted as in Fig. 4. The curves through these data, however, can be

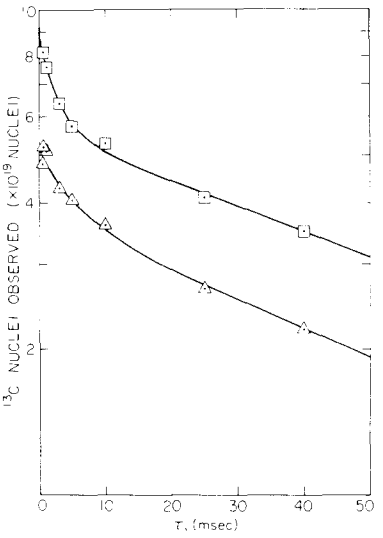

FIG. 4. Amplitude of the observed ^{13}C magnetization versus τ, the delay between the 180 and the 90° pulses, for formic acid adsorbed on the NH_4–Y (⊡) and the ultrastable H–Y (△) zeolites at 295 K. Absolute counts for the ^{13}C nuclei were calibrated with an enriched adamantane sample. The proton decoupling was 16 G.

fit with the sum of two exponentials which has the general form

$$M(\tau) = M_0(\alpha_a e^{-\tau/T_{1a}} + \alpha_b e^{-\tau/T_{1b}}), \quad (1)$$

where M_0 is the equilibrium magnetization and α_a and α_b are the proportions of spins with relaxation times T_{1a} and T_{1b}, respectively. A least-squares fit to the data for the NH_4–Y sample yields $M_0 = 8.8 \times 10^{19}$ ^{13}C nuclei and 35% relax with an average T_1 of about 2.6 msec and 65% relax with an average T_1 of 82 msec. For the ultrastable H–Y sample, $M_0 = 5.2 \times 10^{19}$ ^{13}C nuclei, of which 25% relax with an average T_1 of 4.4 msec and 75% with an average T_1 of 71 msec. The centers-of-mass and the linewidths did not change significantly as τ was lengthened. However, the extremely weak signals for long values of τ caused large experimental error limits, as much as 20 ppm for delays longer than 10 msec.

The lineshapes for two representative ^{13}C NMR spectra resulting from the 180°–τ–90° sequence for formic acid adsorbed on the NH_4–Y and the ultrastable H–Y zeolites at 295 K are shown in Fig. 5. These lineshapes are for short delays, τ = 0.5 msec; thus the two T_1 groups are overlapped in each spectrum. The centers-of-mass of the ^{13}C lineshapes of the adsorbed formic acid are −164 and −165 ppm, relative to TMS, for the NH_4–Y and the ultrastable H–Y sub-

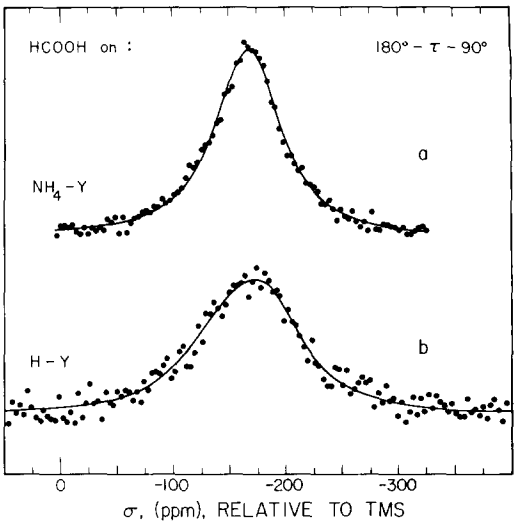

FIG. 5. ^{13}C NMR spectra of formic acid adsorbed on (a) the NH_4–Y zeolite (130,000 averages) and (b) the ultrastable H–Y zeolite (66,000 averages), as measured by the 180°–τ–90° experiment at 295 K. In both spectra, τ = 0.5 msec and proton decoupling was 16 G.

TABLE 2

^{13}C Spectral Parameters of Adsorbed Formic Acid

Spectrum	Experiment	Temperature (K)	Linewidth[a]	Principal components[b]			$\bar{\sigma}$[c]	$\frac{\sigma_{22}-\sigma_{11}}{\sigma_{33}-\sigma_{11}}$	δ[d]
				σ_{11}	σ_{22}	σ_{33}			
			A. HCOOH on the NH_4–Y zeolite						
5a	180°–τ–90°	295	60	−153	−168	−172	−164	0.79	103[e]
8a	cross-polarization	295	75	−129	−151	−161	−147	0.69	124
8b	cross-polarization	150	111	−95	−152	−233	−160	0.41	53
			B. HCOOH on the Ultrastable H–Y zeolite						
5b	180°–τ–90°	295	98	−112	−176	−206	−165	0.68	100[e]
8c	cross-polarization	295	105	−95	−155	−199	−150	0.58	142
8d	cross-polarization	115	144	−98	−145	−240	−161	0.33	116

[a] Full width at half-maximum, in ppm.
[b] In ppm, relative to TMS.
[c] Isotropic frequency of the lineshape, relative to TMS.
[d] Linewidth of the Gaussian broadening function convoluted into the powder pattern, in ppm.
[e] Spectrum convoluted with a Lorentzian broadening function.

strates, respectively. This is within experimental error of pure formic acid: −163 ppm (*46*). The linewidths are comparable to those of the reference formates, but the spectral structures at the principal components of the chemical shift tensor are not as well resolved. Accordingly, the uncertainty in the fitted chemical shift parameters reported in Table 2 are greater; about ±10 ppm.

The 180°–τ–90° experiment does not observe all the ^{13}C originally deposited on the zeolites. The equilibrium magnetization, M_0, accounts for only 89 and 51% of the formic acid on the NH_4–Y and the ultrastable H–Y zeolites, respectively. M_0 remains unchanged when the interval between successive pulse cycles (A and B in Fig. 2) is increased to 10 sec. Thus, the spin-count deficiency is not a saturation artifact. A small portion of the spins (less than about 4%) may be undetectable because the formate molecules are adsorbed within a critical radius of a paramagnetic impurity (about 7 Å). The NMR signals from these species would be extremely broad and thus not observed (*47*).

Another contribution to the spin-count deficiency is suggested by the ^{13}C NMR spectra of the aged samples. The T_1 data and the spectra in Fig. 5 were obtained after the zeolites had been loaded with the formic acid and stored at 273 K for 4 weeks. Figure 6 shows the spectra obtained for the ultrastable H–Y sample after an additional 7 months at 273 K. The intensity of the broad line centered at −165 ppm has decreased significantly and there is a sharp feature at −180 ppm. This sharp line remains even when proton decoupling is not applied, indicating that for this species, the coupling to the protons is less than its linewidth: 150 Hz. Since the isotropic chemical shift of pure CO is −181 ppm (*46*) and CO is the principal reaction product for formic acid on these zeolites, we attribute the sharp peak to a mobile CO species. Therefore, the ^{13}C NMR data indicate that the formic acid is decomposing to CO which desorbs into the dead volume above the NMR sample. This would cause some of the ^{13}C nuclei to be undetected. However, this cannot account for all the unobserved ^{13}C nuclei since one would expect to observe a CO signal in spectrum 5b when almost half of the spins were not detected.

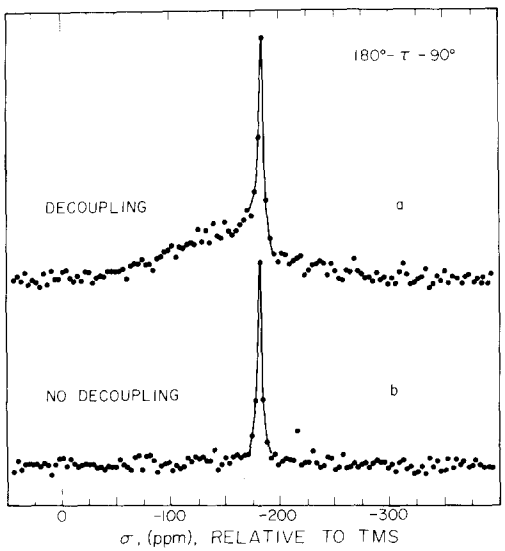

FIG. 6. ^{13}C NMR spectra of the ultrastable H–Y zeolite dosed with formic acid, after 8 months, with (a) 16-G proton decoupling and (b) no decoupling. Both spectra are the result of about 66,000 averages of the 180°–τ–90° sequence with τ = 0.5 msec at 295 K.

2. *Cross-Polarization Experiments*

The ^{13}C NMR signal intensity of the adsorbed formic acid as a function of the cross-polarization time is shown in Fig. 7. The maximum magnetization for both zeolite samples was attained at approximately 0.6 msec. These data were also measured when the samples were 4 weeks old, the same time as the T_1 data in Fig. 4. However, the signal from the ultrastable H–Y sample is greater than the signal from the NH_4–Y sample, although it was a factor of 1.7 less in the 180°–τ–90° experiment. In general, the maximum signal enhancement for the ^{13}C–^1H cross-polarization is a factor of 4, provided that there is an infinite proton spin bath relative to the ^{13}C spins and

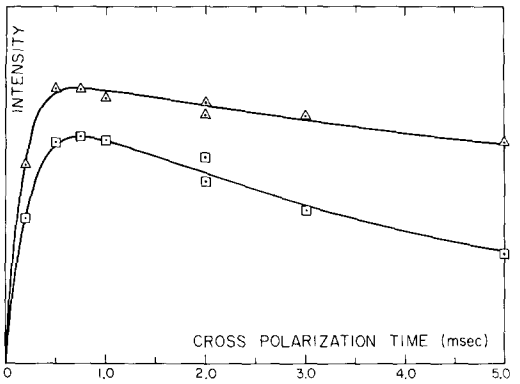

FIG. 7. The amplitude of the observed ^{13}C magnetization versus the length of the cross-polarization process for formic acid adsorbed on the NH_4–Y (⊡) and the ultrastable H–Y (△) zeolites at 295 K. The proton decoupling was 16 G.

the ^{13}C and ^{1}H T_1's are long compared to the time constant of the heteronuclear interaction, T_{IS}. The ratios of the heat capacities of the ^{1}H and ^{13}C baths are 120:1 and 30:1 for the NH_4–Y and ultrastable H–Y zeolites, respectively, sufficient to approximate an infinite bath of ^{1}H spins. The maximum enhancements measured for the adsorbed formic acid are factors of 1.9 and 3.2 for the formic acid adsorbed on the NH_4–Y and ultrastable H–Y samples, respectively. Thus, the ultrastable H–Y sample has an effective ^{13}C–^{1}H magnetization transfer, but the NH_4–Y sample is considerably below the theoretical maximum.

The data in Fig. 7 may be interpreted with the following thermodynamic model. The ^{13}C magnetization increases via transfer of magnetization from the ^{1}H spins. The rate of transfer is proportional to the difference in the spin temperature between the two baths and is determined by the rate constant T_{IS}^{-1}. The ^{13}C magnetization decays by two processes: directly, by relaxation with the lattice, and indirectly, by transfer of magnetization back to the proton bath which, in turn, is directly relaxing with the lattice. Solving the coupled differential equations for the rate of change of the magnetization of the two spin systems and taking the limit of an infinite ^{1}H bath relative to the ^{13}C bath yields

$$M_{xp}(t_{xp}) = \alpha_{xp} M_0 \frac{\gamma_H}{\gamma_C} \left[\frac{T_{1C} T_{1H}}{T_{1C} T_{1H} + T_{IS} T_{1H} - T_{IS} T_{1C}} \right] [e^{-t_{xp}/T_{1H}} - (e^{-t_{xp}/T_{IS}})(e^{-t_{xp}/T_{1C}})]. \quad (2)$$

Thus, the observed ^{13}C magnetization, M_{xp}, a function of the cross-polarization time, t_{xp}, grows exponentially with rate constant $(T_{IS}^{-1} + T_C^{-1})$ and then decreases exponentially with rate constant T_{1H}^{-1}. The values for M_0 have been determined previously with the 180°–τ–90° experiment. The enhancement of the magnetization is determined by the product of three prefactors: a term containing the three rate constants (which is about 1.0), the ratio of the gyromagnetic ratios γ_H/γ_C (which is 4.0), and normalization factor, α_{xp}. In general α_{xp} is the fraction of the ^{13}C nuclei susceptible to the cross-polarization process before the magnetizations decay in the respective holding fields. The physical interpretation of the factor will be discussed later. T_{1C} and T_{1H}, the relaxation times in the respective holding fields, are determined experimentally. The data for formic acid on the NH_4–Y zeolite in Fig. 7 are fit with T_{IS} = 0.23 msec, T_{1H} = 5.6 msec, and T_{1C} = 3.0 msec. The formic acid on the ultrastable H–Y sample is characterized by a shorter T_{IS}, 0.16 msec, indicating a stronger ^{13}C–^{1}H coupling, T_{1H} = 16 msec and T_{1C} = 5.0 msec. These values of T_{IS} are similar to those of the reference formates. The lines are relatively insensitive to the value of T_{1C}. The least-squares fitted values for α_{xp} are 0.52 and 0.83 for the NH_4–Y and ultrastable H–Y samples, respectively.

Typical spectra obtained by observing the proton-decoupled free-induction decays immediately after the ^{13}C holding pulses are shown in Fig. 8. Although the signal-to-noise ratio is considerably better than that of the 180°–τ–90° experiment, the chemical shift components are again not well resolved. The fitted components and lineshape parameters are given in Table 2.

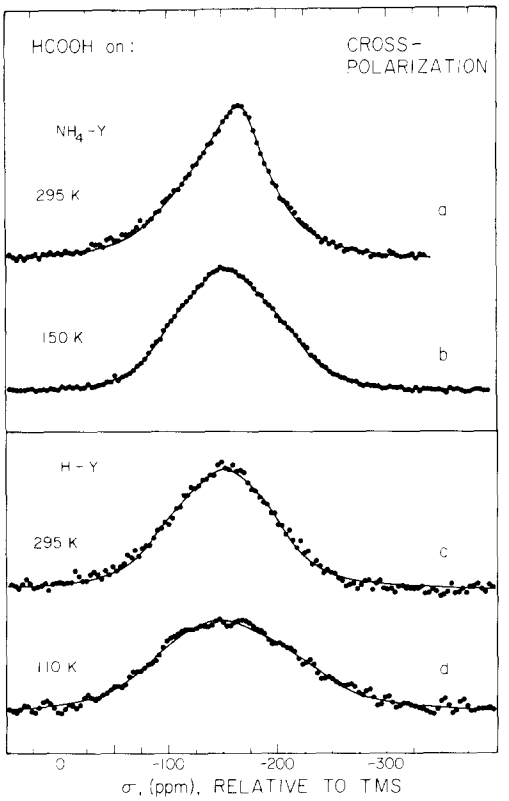

FIG. 8. ^{13}C NMR spectra of adsorbed formic acid as a function of temperature, measured by the cross-polarization scheme. The data were recorded immediately after 1.0 msec of cross-polarization with 16 G of proton decoupling. The spectra are formic acid adsorbed on the NH_4–Y zeolite at (a) 295 K and at (b) 150 K; and on the ultrastable H–Y zeolite at (c) 295 K and at (d) 115 K. Each spectrum is the accumulation of about 66,000 averages.

Compared to the spectra from the 180°–τ–90° experiment, the lineshapes from the cross-polarization experiments are about 25 and 7% broader for the NH_4–Y and the ultrastable H–Y samples, respectively. The increased broadening in the spectra is the result of the cross-polarization process emphasizing the signals from adsorbed species with broader lineshapes. In general, the more stationary formate species will have stronger ^{13}C–^1H couplings and thus will be enhanced more. The internuclear cross-polarization process will be ineffective for rapidly reorienting ^{13}C–^1H systems and these ^{13}C nuclei will be polarized only through ^{13}C–^{13}C homonuclear transfers or intermolecular ^{13}C–^1H couplings. Such processes would require about 5 to 10 msec of cross-polarization, as is necessary for the rapidly tumbling molecules of adamantane at 295 K. For the adsorbed formic acid molecules, such long transfers are not possible since the magnetization in the holding field decays before the process would be complete. Thus, the lineshapes in Fig. 8 are primarily due to adsorbed formic acid molecules with nearly rigid ^{13}C–^1H bond systems.

The spectrum from the NH_4–Y sample broadens the most compared to the 180°–τ–90° spectrum, indicating that it contains a larger percentage of reorienting adsorbed species. The ultrastable H–Y sample has a much smaller change in linewidth. This is consistent with the enhancement factor of 3.2 which suggests that a larger percentage of the formic acid on the ultrastable H–Y sample is rigidly bonded to the substrate.

The center-of-mass frequencies of the cross-polarized spectra at 295 K are 17 and 15 ppm upfield from the 180°–τ–90° spectra for the NH_4–Y and the ultrastable H–Y zeolites, respectively. This also indicates that the cross-polarization technique is emphasizing a specific subgroup of the total lineshape. The isotropic frequencies on both samples at 295 K do not change as a function of the cross-polarization time for the range reported in Fig. 7.

The cross-polarization spectra broaden and the isotropic frequencies move almost back to that of the 180°–τ–90° spectra as the temperature is lowered, as seen in Fig. 8 and Table 2. In addition, the general shapes of the spectra change, which is best visualized for the formic acid adsorbed on the NH_4–Y zeolite. The frequency at which the maximum intensity occurs shifts from the downfield side (i.e., the more negative side) of the isotropic frequency to the upfield side as the temperature is decreased. Spectra were measured at several intermediate temperatures, and it was observed that this shift is a gradual process.

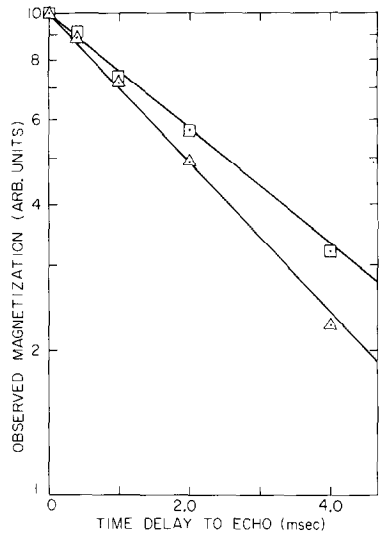

FIG. 9. The amplitude of the observed ^{13}C magnetization versus the delay to the echo in the cross-polarization sequence for formic acid adsorbed on the NH_4–Y zeolite (⊡) and the ultrastable H–Y zeolite (△) at 295 K. Proton-decoupling pulses of 16 G were applied immediately after the ^{13}C spin-locking pulses.

The logarithm of the spectral area as a function of the delay from the end of the ^{13}C cross-polarization holding pulse to the echo for the formic acid adsorbed on the zeolites at 295 K is plotted in Fig. 9. For each zeolite sample, the areas decay with a single transverse relaxation time, T_2. The values of T_2 are 2.5 and 3.1 msec for the formic acid adsorbed on the NH_4–Y and the ultrastable H–Y zeolites, respectively. The center-of-mass frequencies and the linewidths of the spectra do not vary, within experimental limits, as a function of the echo time.

3. *Dipolar-Modulation Experiments*

The heteronuclear dipolar-modulation experiments were performed on the formic acid adsorbed on the NH_4–Y zeolite at both 295 and 125 K. The ^{13}C magnetization was first prepared by cross-polarizing for 1.0 msec. Recall from previous results that the cross-polarization process will enhance selectively the more rigidly adsorbed formic acid molecules. The NMR signal was observed as an echo 1.2 msec after the end of the ^{13}C spin-locking pulse. Since the ^{13}C NMR spectra from the previous experiments do not have a well-resolved structure at the principal chemical shift components, it is not possible to assign the modulations in the lineshapes to distinct molecular orientations as was previously done with benzene and calcium formate (*27, 37*). However, the variation of the spectral area as a function of the number of ^1H eight-pulse cycles (the dipolar-modulation time, see Fig. 2) yields an average dipolar interaction and, thus, information on the average ^{13}C–^1H bond length and the extent of motional averaging (*27*). The spectral areas versus the dipolar-modulation time are shown in Fig. 10. The spectral area of the adsorbed formic acid initially decreases at a rate comparable to that of calcium formate. Also note that the areas of the ^{13}C NMR spectra of calcium formate and benzene exhibit a damped oscillation about zero as predicted, but the spectral areas of adsorbed formic acid remain positive and do not oscillate.

4. *Dipolar-Difference Experiment*

The ultimate dehydration of formic acid necessarily requires the cleavage of the carbon–hydrogen bond. Thus, the ionic character of the carbonyl hydrogen attached to the adsorbed formate species, relative to formic acid, is of interest in the decomposition reaction. The average electron distribution of the hydrogen atom may be determined by measuring its chemical shift properties.

The linewidth of the homonuclear-decoupled ^1H NMR spectrum of the NH_4–Y zeolite at 295 K is about 26 ppm, as measured by the eight-pulse cycle. This broad Gaussian line is the sum of spectra from the hydrogens of the ammonium ions, the crystalline water, and the hydrogen bonded to the carbon of the adsorbed formic acid. The dipolar-difference experiment eliminates the extraneous hydrogen signals and observes only the spectrum of the carbonyl

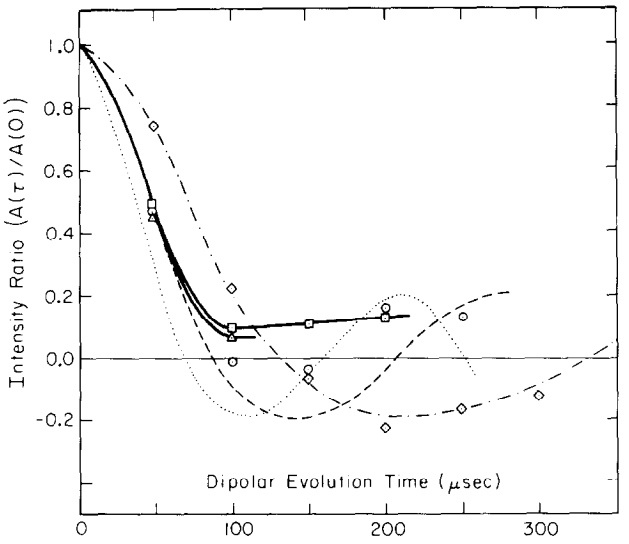

FIG. 10. Spectral areas versus the dipolar-modulation time for formic acid adsorbed on the NH_4–Y zeolite at 295 K (⊡) and at 125 K (△). For comparison, the data for benzene at 185 K (◈) and calcium formate at 295 K (⊙) reported by Stoll *et al.* (*27, 37*) are plotted. Theoretical curves are for a rigid ^{13}C–^1H bond length of 1.09 Å (dotted line), a rigid bond at 1.19 Å (dashed line), and a 1.09-Å bond averaged by rotation in a plane (dashes and dots).

hydrogen, approximately 3% of the total spectrum intensity.

The ^1H NMR spectrum of the carbonyl hydrogen measured by the dipolar-difference experiment at 295 K for the formic acid adsorbed on the NH_4–Y zeolite is shown in Fig. 11. It is similar to the ^{13}C NMR spectra in that it lacks any sharp structure but, in contrast, is much narrower, only 6.0 ppm wide at half-maximum intensity. The center-of-mass frequency for the spectrum is about −12.3 ppm, relative to TMS. Though this experiment may not be calibrated a priori for an unknown system, the spectrum intensity indicates that the number of hydrogen species is on the order of the number of formate species.

IV. DISCUSSION

A. The Nature of the Adsorption of Formic Acid

The adsorption isotherm indicates that submonolayer coverages of formic acid are chemically adsorbed on the zeolites. As will be discussed, the ^{13}C NMR spectra indicate that the formate species are immobile on the surface, though there is some motion localized at a site.

The ^{13}C NMR linewidths of the adsorbed formic acid are comparable to that of the solid reference formates. In general, the linewidth of the NMR spectrum of an adsorbed species may be the result of a number of interactions including paramagnetic broadening, heteronuclear dipolar broadening (from nuclei other than ^1H), spatial

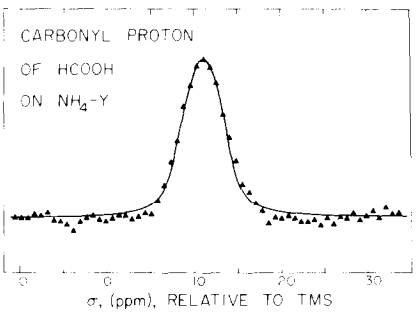

FIG. 11. ^1H NMR spectrum of the carbonyl hydrogen of formic acid adsorbed on the NH_4–Y zeolite at 295 K, obtained with about 8000 averages of the dipolar-difference experiment.

susceptibility inhomogeneities, and chemical shift anisotropy. These interactions have been discussed at length elsewhere (*16–18, 48*). The dipolar interactions are the result of the molecular surroundings, such as the framework atoms of the zeolite supercage. The chemical shift broadening is an individual effect, determined by the electron distribution localized at the nucleus of interest.

Of the possible interactions, all *but* the chemical shift anisotropy can be eliminated by considering the ^1H spectrum of the carbonyl proton. If the other effects were the major causes of the ^{13}C NMR linewidth, the ^1H NMR spectrum would also be subjected to these effects and thus would be comparably broadened. However, the linewidth of the ^1H line is only 6 ppm, which places an approximate upper limit on the residual broadening of the ^{13}C NMR spectra.

Thus, the widths of the ^{13}C spectra are due primarily to chemical shift anisotropy. Such anisotropies are observed only for immobile adsorbed states, i.e., the residence times are much longer than the reciprocal linewidth; about 1 msec. (However, there may still exist local motions at a site, as will be discussed later.) If a portion of the formic acid was physically adsorbed on the zeolite, the ^{13}C NMR line would contain an extremely narrowed component, as was observed for the CO decomposition product in Fig. 6.

B. Spin–Lattice Relaxation Times of Adsorbed Formic Acid

In many solids, particularly for ^1H spin systems, the homonuclear spin–spin coupling is much stronger than the spin–lattice coupling. Thus, the macroscopic magnetization decays uniformly and exponentially with time constant T_1. However, in dilute spin systems, the internuclear coupling is weak and each spin relaxes independently. For a dilute homogeneous system, the spins may still have a single T_1 since the spins are relaxing independently, but identically. However, if each spin should relax differently because of different local environments (e.g., paramagnetic impurities or nearby heteronuclear spins or different motional properties), there would be a distribution of relaxation times in the sample. Such T_1 distributions are present in solid $C_6H_5CF_3$ because of an angular dependence of the heteronuclear coupling (*49*) and in CO on Rh on Al_2O_3 due to adsorption site heterogeneity (*21*).

The ^{13}C T_1 data of the formic acid adsorbed on the zeolites may be interpreted by assuming that the formic acid has adsorbed in two states, each described by a different T_1. The relative proportions of the two states are given by the preexponential factors in Eq. (1). Both T_1's on either zeolite are extremely short compared to neat organic compounds and are typical of relaxation by a paramagnetic center. This is consistent with the Fe^{2+} content of 780 ppm which yields an average internuclear distance between the ^{13}C and the Fe nuclei of about 20 Å. It is possible that the two T_1 groups represent chemically different formate species on the surface or that the T_1 distribution is the result of an inhomogeneous distribution of separations between the ^{13}C nuclei and the paramagnetic centers. The change in distributions between the short and long T_1's from the NH_4–Y to the ultrastable H–Y sample (35 : 65 to 25 : 75) is accompanied by an increase in the percentage of ^{13}C spins that are enhanced by the cross-polarization technique. As will be discussed in the next section, this suggests a chemical basis for the different T_1's. On the other hand, the transformation of the NH_4–Y zeolite to the ultrastable H–Y zeolite may have redistributed the paramagnetic centers which would also change the distribution of T_1's.

The spectra from the T_1 experiment associated with the data in Fig. 4 did not change in width or isotropic frequency as τ was increased. However, the signal-to-noise ratios for the spectra with τ longer than about 10 msec became quite poor. Thus, if subtle

changes in either quantity did occur, it would be difficult to detect. Recall that the isotropic chemical shifts for the entire range of formates do not vary more than about 8 ppm. Thus, although the T_1 data suggest a heterogeneity of surface states, it cannot be determined that the sites with different T_1's are chemically distinct.

The nature of the undetected ^{13}C nuclei is indeterminate with the present data. The decomposition to CO accounts for some of the loss. However, it is necessary to study the adsorption of CO on fresh zeolites and zeolites precovered with formic acid to determine why there was no evidence of CO in Fig. 5.

C. Cross-Polarization Experiments

The cross-polarization experiments also indicate that the formic acid is inhomogeneously adsorbed on the zeolites although in this case the basis for the differences may be determined unambiguously. The molecules are differentiated by the rate in which they cross-polarize, that is, by the strength of the dipolar coupling. The spectra shown in Figs. 8a and 8c, observed after 1.0 msec of cross-polarization at 295 K, contain contributions from only those ^{13}C–^{1}H systems with semirigid internuclear vectors. Those systems averaged by reorientations faster than the heteronuclear coupling (about 5 kHz) would require more than 5 msec to complete an intermolecular cross-polarization.

On the ultrastable H–Y zeolite, the intensity of cross-polarized ^{13}C NMR signal was a factor of 3.2 greater than the signal from the 180°–τ–90° experiment. The NH_4–Y sample was enhanced by only a factor of 1.9. These data may be interpreted by assumming that the zeolite contains at least two types of species: those that may be enhanced by the cross-polarization process to the theoretical maximum (a factor of 4) and those that are not cross-polarized in 1.0 msec. With this assumption, the intensities of the cross-polarization spectra indicate that the distribution between the two groups is 52 : 48 on the NH_4–Y zeolite and 83 : 17 on the ultrastable H–Y zeolite. In order to interpret the two types of species, the chemical shift data must be considered.

D. The Relation of Chemical Shift Data to Formate Structures

The formate group bonds in a range of configurations from the ester-like unidentate compounds (species **I**) covalently bonded through a single oxygen atom, to the bidentate structure where the formate ion is chelated about one or more metal ions (species **II** and **III**). The structural parameters of a few compounds are listed in Table 1B. One index of the bonding of the formate group is the ratio of the two carbon–oxygen bond lengths. This ratio ranges from 1.12 for methyl formate to about 1.00 for calcium formate.

The chemical shift information for these formate compounds is presented in Table 1A. The isotropic chemical shifts of the compounds, $\bar{\sigma}$, do not correlate with the geometry of the formate group. This was first observed by Ackerman *et al.* in a study of the two crystallographically distinct forms of calcium formate (*29*). The overall anisotropy, $\sigma_{33} - \sigma_{11}$, tends to decrease as R_2/R_1 decreases, but the scatter in the correlation is extremely large. There is, however, a good correlation between the position of the central principal component, σ_{22}, and the ratio of the carbon–oxygen bond lengths. As the bond lengths become more symmetric, σ_{22} moves from the upfield side of the powder pattern to the downfield side. This is reflected in the ratio of the difference between the upfield component and the central component, $\sigma_{22} - \sigma_{11}$, to the overall anisotropy, $\sigma_{33} - \sigma_{11}$. This ratio ranges from 0.20 for methyl formate ($R_2/R_1 = 1.12$) to 0.66 for calcium formate ($R_2/R_1 = 1.00$). Thus, in general, for bidentate formate ions $(\sigma_{22} - \sigma_{11})/(\sigma_{33} - \sigma_{11})$ is on the order of 0.6, and for ester-like formate groups the ratio is closer to 0.3. As this correlation is based on relatively few data points, the relation between

these two parameters does not permit a reliable calculation of R_2/R_1 from the chemical shift components, only the general trend.

E. The Molecular Structure of the Adsorbed Formic Acid

The relation between the chemical shift components of the ^{13}C NMR spectra and the symmetry of the formate group may be used to determine the state of the adsorbed formic acid. The chemical shift components are meaningful only in ^{13}C powder patterns without appreciable motional averaging. The spectra from the 180°–τ–90° experiment at 295 K, which contain motionally averaged contributions, are not applicable. However, the cross-polarization experiment observes selectively the more rigid species for short cross-polarization times, i.e., about 1.0 msec. Thus, the rigid components of the 180°–τ–90° spectra at 295 K in Fig. 5, isolated by the cross-polarization technique, are shown in Fig. 8. The values of the ratio $(\sigma_{22} - \sigma_{11})/(\sigma_{33} - \sigma_{11})$ for the cross polarized spectra at 295 K for the formic acid adsorbed on the NH_4–Y and ultrastable H–Y zeolites are 0.69 and 0.58, respectively. These relatively high values of this ratio argue that this species is a semirigidly bonded formate ion, with approximately symmetric carbon–oxygen bond lengths. Furthermore, the degree of enhancement of the cross-polarization technique, discussed earlier, indicates that this bidentate species comprises 52 and 83% of the formic acid adsorbed on the NH_4–Y and ultrastable H–Y zeolites, respectively.

When the cross-polarization experiment is repeated at reduced temperatures, the central component of the powder patterns shifts from the downfield side to the upfield side, as mentioned earlier. Specifically, the ratio $(\sigma_{22} - \sigma_{11})/(\sigma_{33} - \sigma_{11})$ changes from 0.69 to 0.41 on the NH_4–Y sample and from 0.58 to 0.33 on the ultrastable H–Y sample. These transitions may be attributed in part to a quenching of the motions responsible for the averaging of the other species at room temperature. If the motionally averaged group had a $(\sigma_{22} - \sigma_{11})/(\sigma_{33} - \sigma_{11})$ ratio comparable to unidentate formate groups, about 0.20, the incorporation of this species into the powder pattern would lower the average ratio. However, on both samples the added contributions from this species do not account for the large decreases in the ratios. For example, since 83% of the formic acid on the ultrastable H–Y zeolite is adsorbed as formate ions, the contribution from the remaining 17% is not sufficient to cause $(\sigma_{22} - \sigma_{11})/(\sigma_{33} - \sigma_{11})$ to decrease from 0.58 to 0.33. One interpretation of the large change is that upon cooling to temperatures below 150 K, some of the surface formate structures convert from bidentate to unidentate structures. This interpretation is supported by the fact that upon cooling, the isotropic chemical shift does not return to the value measured by the 180°–τ–90° experiment. However, because of the lack of pronounced features in the powder patterns, the fitted chemical shift components may be somewhat arbitrary, that is, changing any of the components by 10 ppm will not cause a large change in the error of the fitted spectrum. Thus, there may be errors as large as 25% in the computed ratios and the incorporation of the unidentate species may actually be sufficient to explain the shifts.

Regardless of the exact ratios, there is a definite change in the symmetries of the cross-polarization spectra upon cooling from 295 K to below 150 K. This transition is probably due to the addition of the unidentate groups which have become more rigidly adsorbed at the lower temperature. There may also be some conversion of bidentate ions to unidentate groups although this interpretation will require further study.

F. The Nature of the Bidentate Formate Ion Surface Species

As discussed in the Introduction, the

ultrastable H–Y zeolite is catalytically more active than the NH_4–Y zeolite. Based on the ^{13}C NMR data, the ultrastable H–Y zeolite also has a much higher percentage of the formic acid adsorbed as bidentate groups. This correlation implies that the bidentate group may decompose more readily than the unidentate group. Thus, the nature of this adsorbed state is of interest. By isolating the ^{13}C NMR signal of the bidentate species with the cross-polarization process at 295 K, it is possible to determine the adsorption site, the ^{13}C–^{1}H characteristics, and the ionic character of the carbonyl hydrogen.

In the presence of proton decoupling, the main sources of broadening of the ^{13}C NMR spectra are chemical inhomogeneity of the species, librational motion, lifetime broadening, and dipolar broadening from the ^{27}Al. The full widths at half-maximum of the Gaussian broadening functions convoluted with the chemical shift powder pattern of the cross-polarization spectra at 295 K, spectra 8a and 8c, are 124 and 142 ppm for the NH_4–Y and ultrastable H–Y samples, respectively. The second moments of these broadening functions are 0.67 and 0.88 G^2, respectively. The contributions due to chemical inhomogeneities and librational motions are estimated from the broadening in the reference formates, which is about 0.08 G^2. The lifetime broadenings, computed from the T_2's, are 0.14 G^2 for the NH_4–Y and 0.09 G^2 for the ultrastable H–Y samples. The remainder of the broadening is attributed to the ^{13}C–^{27}Al dipolar interaction. The second moment of this interaction may be calculated from the Van Vleck equation for heteronuclear broadening (*50*):

$$\langle \Delta\omega^2 \rangle_{IS} = \frac{1}{3}\gamma_s^2\hbar^2 s(s+1)\frac{1}{N}\sum_{j,k}\frac{(1-3\cos^2\theta_{jk})}{r_{jk}^6}. \quad (3)$$

In Eq. (3), the second moment of the ^{13}C spectrum due to ^{27}Al is determined by the gyromagnetic ratio of ^{27}Al, 6.97×10^3 rad G^{-1} sec^{-1}; $\hbar$, 1.05×10^{-3} G^2 $Å^3$ sec; the spin of the ^{27}Al nucleus, $S = \frac{5}{2}$; and the ^{13}C–^{27}Al internuclear vector of length r at an angle θ with the external magnetic field. The sum is over all ^{13}C and ^{27}Al spins in the sample, normalized by N, the number of ^{13}C spins. For a polycrystalline sample, the spherical average of the angular dependence is $\frac{4}{5}$. It is assumed that for a formate ion bonded to an Al ion, the bidentate is similar to the Na, Ca, and Sr salts, and the ^{13}C–^{27}Al internuclear distance is 2.75 Å. With this configuration, Eq. (3) yields a second moment of 0.29 G^2. The contribution from Al atoms in the surrounding zeolite framework, not directly bonded to the formate ion, is estimated to be about 0.15 G^2. Thus, the ^{13}C–^{27}Al broadening is calculated to be 0.44 G^2 for a formate ion directly bonded to an Al atom and 0.15 G^2 when bonded to a Si atom.

However, this interaction will increase if the ^{27}Al nuclei are in a non-Zeeman state. That is, it is possible that the orientation of the quadrupolar ^{27}Al nucleus is determined by large electrostatic field gradients at the surface of the zeolite rather than by the external magnetic field. It has been observed that for amorphous aluminas, the ^{27}Al $\frac{1}{2} \longleftrightarrow -\frac{1}{2}$ transition vanishes in samples with BET surface areas greater than about 100 m^2/g, indicating that the ^{27}Al nuclear alignment is determined by local electrostatic fields (*51*). In the case of spin-$\frac{1}{2}$–spin-$\frac{7}{2}$ systems if the spin $\frac{7}{2}$ is in a non-Zeeman state, the spin-$\frac{1}{2}$ second moment may increase by as much as a factor of 1.8 (*52*). Similarly, it has been shown that the non-Zeeman state of ^{27}Al (spin $\frac{5}{2}$) may also increase the contribution to the spin-$\frac{1}{2}$ second moment by a factor as large as 1.8 (*53*). Thus, the total second moment, including the librational contribution, is about 0.52 to 0.87 G^2 for the formate ion bonded directly to the Al atom and about 0.23 to 0.35 G^2 for the formate ion bonded to an Si atom. The second moments of the observed broadenings of the chemical shift powder patterns,

minus the lifetime contributions are 0.53 G^2 for the NH_4–Y sample and 0.79 G^2 for the ultrastable H–Y sample. Thus, the residual dipolar broadening indicates that the formate ion is bonded to the Al ions.

The dipolar-modulation data for the formate ion on the NH_4–Y zeolite, shown in Fig. 10, indicate that the ^{13}C–^1H coupling is similar to that of calcium formate. The initial decrease of the spectral area for both calcium formate and the surface formate ion is less than predicted for a bond length of 1.09 Å, shown by the dotted line in Fig. 10. The bond length in calcium formate measured by X-ray diffraction is 1.09 Å. The slower initial decrease in the spectral area compared to the theoretical rate has been attributed to librational motions of the calcium formate (*27, 37*). We propose that the ^{13}C–^1H bond length of the adsorbed formate ion is also 1.09 Å and is undergoing motions similar to those in calcium formate. As the dipolar-modulation time is increased, the spectral area of the adsorbed formic acid does not decrease below zero, contrary to the data of calcium formate and solid benzene. It is suggested that although the direct ^1H–^1H coupling is suppressed by the eight-pulse cycles, the ^1H nuclei are still indirectly coupled through the ^{27}Al nuclei. Thus, after about 0.1 msec, the ^1H–^{27}Al–^1H spin diffusion has destroyed some of the phase coherence in the experiment.

Analogous to the cross-polarization experiments, the dipolar-difference technique observes only those hydrogen nuclei with strong heteronuclear dipolar couplings. That is, the dipolar-difference method isolates the hydrogens bonded to ^{13}C nuclei with little motional averaging. Thus, the ^1H spectrum in Fig. 11 is assigned to the carbonyl proton of the bidentate formate ion on the NH_4–Y zeolite at 295 K. As was discussed earlier, the ionic character of this proton is of importance to dehydration reaction mechanisms. The isotropic chemical shift of this spectrum, −12.3 ppm relative to TMS, is similar to that of formate salts. It has been reported previously that the corresponding protons in calcium formate and ammonium formate have isotropic chemical shifts of −10.9 and −12.8 ppm, whereas formic acid is further upfield, at −9.2 ppm (*28*). The downfield shift of the chemical shift of the carbonyl hydrogen suggests that the hydrogen has acquired a more acidic nature. Thus, the hydrogen may be more susceptible to nucleophilic attack, or it may shift more readily to electron-rich centers.

V. CONCLUSIONS

Several multiple-pulse NMR techniques have been applied to measure the dipolar interactions, spin-relaxation rates, and chemical shift properties of formic acid adsorbed on an NH_4–Y and an ultrastable H–Y zeolite. The results indicate that the formic acid is chemically adsorbed into two immobile states which are differentiated by the strength of the ^{13}C–^1H dipolar coupling. The ^{13}C chemical shift tensor of the more rigidly held species, observed selectively by cross-polarization techniques at 295 K, has a symmetry similar to the spectra of inorganic formate salts with bidentate structures. The other surface species is assigned to a unidentate structure. From the enhancements obtained by the cross-polarization technique, relative to the 180°–τ–90° experiment, it is determined that the ratio of bidentate to unidentate groups is 52 : 48 on the NH_4–Y zeolite and 83 : 17 on the ultrastable H–Y zeolite. These values are for coverages of about 0.3 monolayer on both the NH_4–Y and the ultrastable H–Y zeolites.

The formate adsorbed in a bidentate form, which may be more reactive than the unidentate, was further quantified with the NMR techniques. The magnitude of the broadening in the ^{13}C NMR spectra that can be attributed to ^{27}Al dipolar interactions indicates that the bidentate formate group is bonded to an Al atom. The dipolar-modulation spectra of the bidentate species suggest that the ^{13}C–^1H bonding is similar to

formate salts, such as calcium formate. The carbonyl hydrogen has become more acidic upon adsorption into the bidentate state, as reflected by the downfield shift of the center-of-mass of the ^1H NMR spectrum. This increased acidity is possibly related to the cleavage mechanism of the carbon–hydrogen bond. Conversely, the ^{13}C center-of-mass of the bidentate species is shifted upfield relative to neat formic acid and formate salts, by at least 15 ppm. However, because of the complex combination of the paramagnetic and diamagnetic contributions to the chemical shift, it is not possible to interpret this shift in terms of the ionic state of the carbon atom.

The motional averaging of the unidentate group is most likely a reorientation at the adsorption site, such as rotation about the bond between the oxygen and the adsorption site or the carbon–oxygen bond. It is conceivable that the different bonding to the zeolite surface is the result of formic acid bonding to Si atoms.

As discussed in the Introduction, it has been proposed that the thermal decomposition of the NH_4–Y zeolite to the ultrastable H–Y zeolite is accompanied by the extraction of 9 to 15 Al cations from the zeolite framework (*10*). This proposal is consistent with the increased proportion of bidentate formate groups on the ultrastable H–Y zeolite. In addition, the average ^{13}C–^{27}Al dipolar coupling for the bidentate groups is stronger on the ultrastable H–Y zeolite, as evidenced by a 50% increase in the second moment of the interaction.

Multiple-pulse NMR techniques can isolate and quantify the various interactions in the nuclear environment of adsorbed molecules. This information, considered with respect to the results of electronic and vibrational spectra, can differentiate and further quantify the adsorbed states. Additional NMR techniques tailored to the analysis of dilute catalytic systems, and the probing of other nuclei, such as ^{27}Al or ^{29}Si, will increase the capabilities of this approach to catalytic studies.

ACKNOWLEDGMENTS

This work was supported in part by the Office of Naval Research, under Contract N00014-75-0960. The authors wish to thank J. A. Reimer for obtaining the dipolar-modulation and dipolar-difference spectra, G. W. Brudvig for measuring the electron paramagnetic spectra of the zeolites, and Dr. G. T. Kerr of Mobil Research and Development Corporation for supplying the zeolite samples. We also are indebted to Professor S. I. Chan for helpful discussions and comments.

REFERENCES

1. Hirota, K., Fueki, K., Shindo, K., and Nakai, Y., *Bull. Chem. Soc. Japan* **32,** 1261 (1959).
2. Scholten, J. J. F., Mars, P., Menon, P. G., and van Hardeveld, R., *in* "Proceedings, 3rd International Congress on Catalysis, Amsterdam, 1964," p. 881. North-Holland, Amsterdam, 1964.
3. Bielański, A., and Datka, J., *J. Catal.* **32,** 183 (1974).
4. Noto, Y., Fukuda, K., Onishi, T., and Tamaru, K., *Trans. Faraday Soc.* **63,** 2300 (1967).
5. Lewis, B. F., Mosesman, M., and Weinberg, W. H., *Surface Sci* **41,** 142 (1974).
6. Shklyarevskii, O. I., Lysykh, A. A., and Yanson, I. K., *Sov. J. Low Temp. Phys.* **2,** 328 (1976).
7. Venuto, P. B., and Landis, P. S., *Advan. Catal.* **18,** 259 (1968).
8. (a) Kerr, G. T., *Advan. Chem. Ser.* **121,** 219 (1973); (b) McDaniel, C. V., and Maher, P. K., *in* "Molecular Sieves," p. 86. Soc. Chem. Ind., London, 1968.
9. Poutsma, M. L., *in* "Zeolite Chemistry and Catalysis" (J. A. Rabo, Ed.), p. 437, Amer. Chem. Soc. Monogr. 171. Amer. Chem. Soc., Washington, D.C., 1976.
10. Kerr, G. T., *J. Catal.* **15,** 200 (1969).
11. Smith, J. V., *in* "Zeolite Chemistry and Catalysis" (J. A. Rabo, Ed.), p. 56, Amer. Chem. Soc. Monogr. 171. Amer. Chem. Soc., Washington, D.C., 1976.
12. Theimer, R., and Theimer, O., *Monatsh.* **81,** 313 (1950).
13. Ellis, B., and Pyszora, H., *Nature (London)* **181,** 181 (1958).
14. Kagarise, R. E., *J. Phys. Chem.* **59,** 271 (1955).
15. Hall, J. T., and Hansma, P. K., *Surface Sci.* **76,** 61 (1978).
16. Derouane, E. G., Fraissard, J., Fripiat, J. J., and Stone, W. E. E., *Catal. Rev.* **7,** 121 (1972).
17. Pfeifer, H., *in* "NMR—Basic Principles and Progress" (P. Diehl, E. Fluck, and R. Kosfeld, Eds.), Vol. 7, p. 55. Springer-Verlag, New York, 1972.
18. Delgass, W. N., Haller, G. L., Kellerman, R., and Lunsford, J. H., "Spectroscopy in Heterogeneous Catalysis." Academic Press, New York, 1979.

19. Kaplan, S., Resing, H. A., and Waugh, J. S., *J. Chem. Phys.* **59,** 5681 (1973).
20. Stejskal, E. O., Schaefer, J., Henis, J. M. S., and Tripoli, M. K., *J. Chem. Phys.* **61,** 2351 (1974).
21. Duncan, T. M., Yates, J. T., Jr., and Vaughan, R. W., *J. Chem. Phys. 73,* 975 (1980).
22. Vaughan, R. W., *Annu. Rev. Phys. Chem.* **29,** 397 (1978).
23. Mehring, M., "High Resolution NMR Spectroscopy in Solids, NMR—Basic Principles and Progress" (P. Diehl, E. Fluck, and R. Kosfeld, Eds.), Vol. 11, p. 1. Springer-Verlag, New York, 1976.
24. Haeberlin, U., "High Resolution NMR in Solids—Selective Averaging," Advances in Magnetic Resonance, Suppl. 1, (J. S. Waugh, Ed.). Academic Press, New York, 1976.
25. (a) Pines, A., Gibby, M. G., and Waugh, J. S., *J. Chem. Phys.* **56,** 1776 (1972); (b) Pines, A., Gibby, M. G., and Waugh, J. S., *J. Chem. Phys.* **59,** 569 (1973).
26. Demco, D. E., Tegenfeldt, J., and Waugh, J. S., *Phys. Rev. B* **11,** 4133 (1975).
27. (a) Stoll, M. E., Vega, A. J., and Vaughan, R. W., *J. Chem. Phys.* **65,** 4093 (1976); (b) Stoll, M. E., Vega, A. J., and Vaughan, R. W., XIX Congress Ampere, Heidelberg, 1976.
28. Reimer, J. A., and Vaughan, R. W., *Chem. Phys. Lett.* **63,** 163 (1979).
29. Ackerman, J. L., Tegenfeldt, J., and Waugh, J. S., *J. Amer. Chem. Soc.* **96,** 6843 (1974).
30. Al'tshuler, S. A., and Kozyrev, B. M., "Electron Paramagnetic Resonance in Compounds of Transition Elements," 2nd ed. (translated from Russian). Wiley, New York, 1974.
31. Coolidge, A. S., *J. Amer. Chem. Soc.* **50,** 2166 (1928).
32. McDaniel, C. V., and Maher, P. K., *in* "Zeolite Chemistry and Catalysis" (J. A. Rabo, Ed.), p. 296, Amer. Chem. Soc. Monogr. 171. Amer. Chem. Soc., Washington, D.C., 1976.
33. Vaughan, R. W., Elleman, D. D., Stacey, L. M., Rhim, W. K., and Lee, J. W., *Rev. Sci. Instrum.* **43,** 1356 (1972).
34. Stoll, M. E., Vega, A. J., and Vaughan, R. W., *Rev. Sci. Instrum.* **48,** 800 (1977).
35. (a) Carr, H. Y., and Purcell, E. M., *Phys. Rev.* **49,** 630 (1954); (b) Vold, R. L., Waugh, J. S., Klein, M. P., and Phelps, D. E., *J. Chem. Phys.* **48,** 3831 (1968).
36. Hartmann, S. R., and Hahn, E. L., *Phys. Rev.* **128,** 2042 (1962).
37. Stoll, M. E., Ph.D. thesis, California Institute of Technology, 1977.
38. Rhim, W. K., Elleman, D. D., Schreiber, L. B., and Vaughan, R. W., *J. Chem. Phys.* **60,** 1595 (1974).
39. Mehring, M., Pines, A., Rhim, W. K., and Waugh, J. S., *J. Chem. Phys.* **54,** 3239 (1971).
40. Bloembergen, N., and Rowland, J. A., *Acta Metall.* **1,** 731 (1953).
41. Pines, A., Gibby, M. G., and Waugh, J. S., *Chem. Phys. Lett.* **15,** 373 (1972).
42. O'Gorman, J. M., Shand, W., Jr., and Schomaker, V., *J. Amer. Chem. Soc.* **72,** 4222 (1950).
43. Lerner, R. G., Dailey, B. P., and Friend, J. P., *J. Chem. Phys.* **26,** 680 (1957).
44. Nahringbauer, I., *Acta Crystallogr. Sect. B* **24,** 565 (1968).
45. Nitta, I., and Osaki, K., *X-Rays* **5,** 37 (1948); ref. in "Structural Reports," Vol. 11, p. 556, 1948.
46. Stothers, J. B., "Carbon-13 NMR Spectroscopy." Academic Press, New York, 1972.
47. Abragam, A., "The Principles of Nuclear Magnetism," Chap. IX. Oxford University Press, London, 1961.
48. Sefcik, M. D., Schaefer, J., and Stejskal, E. O., *in* "Molecular Sieves II" (J. R. Katzer, Ed.), p. 344, Amer. Chem. Soc. Symp. Ser. 40. Amer. Chem. Soc., Washington, D.C., 1977.
49. Anderson, J. E., and Slichter, W. P., *J. Chem. Phys.* **43,** 433 (1965).
50. Reference (47), Chap. IV.
51. (a) O'Reilly, D. E., *J. Chem. Phys.* **28,** 1263 (1958); (b) O'Reilly, D. E., *Advan. Catal.* **12,** 31 (1960).
52. Vanderhart, D. L., Gutowsky, H. S., and Farrer, T. C., *J. Amer. Chem. Soc.* **89,** 5056 (1967).
53. Vanderhart, D. L., Ph.D. thesis, University of Illinois, 1968.